

Ultra-low Young's modulus and high super-exchange interactions in monolayer CrN: A promising candidate for flexible spintronic applications

Yang Song(宋洋), Yan-Fang Zhang(张艳芳), Jinbo Pan(潘金波), and Shixuan Du(杜世萱)
Citation: Chin. Phys. B, 2021, 30 (**4**): 047105. DOI: 10.1088/1674-1056/abdb20
Journal homepage: http://cpb.iphy.ac.cn; http://iopscience.iop.org/cpb

What follows is a list of articles you may be interested in

Two-dimensional hexagonal Zn_3Si_2 monolayer: Dirac cone material and Dirac half-metallic manipulation

Yurou Guan(官雨柔), Lingling Song(宋玲玲), Hui Zhao(赵慧), Renjun Du(杜仁君), Liming Liu(刘力铭), Cuixia Yan(闫翠霞), Jinming Cai(蔡金明)
Chin. Phys. B, 2020, 29 (**8**): 087103. DOI: 10.1088/1674-1056/ab943a

A review of current research on spin currents and spin-orbit torques

Xiao-Yu Feng(冯晓玉), Qi-Han Zhang(张琪涵), Han-Wen Zhang(张瀚文), Yi Zhang(张祎), Rui Zhong(钟瑞), Bo-Wen Lu(卢博文), Jiang-Wei Cao(曹江伟), Xiao-Long Fan(范小龙)
Chin. Phys. B, 2019, 28 (**10**): 107105. DOI: 10.1088/1674-1056/ab425e

Metal-to-insulator transition in two-dimensional ferromagnetic monolayer induced by substrate

Can Qi(齐灿), Jun Hu(胡军)
Chin. Phys. B, 2018, 27 (**7**): 077106. DOI: 10.1088/1674-1056/27/7/077106

Investigations of the half-metallic behavior and the magnetic and thermodynamic properties of half-Heusler CoMnTe and RuMnTe compounds：A first-principles study

T. Djaafri, A. Djaafri, A. Elias, G. Murtaza, R. Khenata, R. Ahmed, S. Bin Omran, D. Rached
Chin. Phys. B, 2014, 23 (**8**): 087103. DOI: 10.1088/1674-1056/23/8/087103

The electronic and magnetic properties of (Mn,C)-codoped ZnO diluted magnetic semiconductor

Zhao Long, Lu Peng-Fei, Yu Zhong-Yuan, Ma Shi-Jia, Ding Lu, Liu Jian-Tao
Chin. Phys. B, 2012, 21 (**9**): 097103. DOI: 10.1088/1674-1056/21/9/097103

Ultra-low Young's modulus and high super-exchange interactions in monolayer CrN: A promising candidate for flexible spintronic applications*

Yang Song(宋洋), Yan-Fang Zhang(张艳芳)†, Jinbo Pan(潘金波), and Shixuan Du(杜世萱)

Institute of Physics and School of Physical Sciences, University of Chinese Academy of Sciences, Chinese Academy of Sciences, Beijing 100190, *China*

(Received 10 October 2020; revised manuscript received 11 December 2020; accepted manuscript online 13 January 2021)

Monolayer CrN has been predicted to be half-metallic ferromagnet with high Curie temperature. Due to bulk CrN's biocompatibility, the monolayer is a promising candidate for bio-related devices. Here, using first-principles calculations based on density functional theory, we find that the formation energy of the bulk CrN stacking from layers with square lattice is only 68 meV/atom above the convex hull, suggesting a great potential to fabricate the monolayer CrN in a square lattice by using molecular beam epitaxy method. The monolayer CrN is then proved to be a soft material with an ultra-low Young's modulus and can sustain very large strains. Moreover, the analysis of the projected density of states demonstrates that the ferromagnetic half-metallicity originates from the splitting of Cr-d orbitals in the CrN square crystal field, the bonding interaction between Cr–N, and that between Cr–Cr atoms. It is worth noting that the super-exchange interaction is much larger than the direct-exchange interaction and contributes to the ultra-high Curie temperature, which is obtained from Monte Carlo simulations based on Heisenberg model. Our findings suggest that the monolayer CrN can be an indispensable candidate for nanoscale flexible spintronic applications with good biocompatibility and is considerable appealing to be realized in experiment.

Keywords: monolayer CrN, half-metallic ferromagnet, flexible material, spintronics

PACS: 71.20.Gj, 62.20.de, 81.40.Jj, 75.50.Dd **DOI:** 10.1088/1674-1056/abdb20

1. Introduction

Inspired by the first successful exfoliation of graphene from graphite in 2004,[1] two-dimensional (2D) materials are of wide interest for their promising application potentials in nanoscale devices owing to a wide range of superior properties from electrical, such as insulating,[2] semiconducting,[3,4] Dirac-metallic,[5,6] half-metallic,[7,8] metallic,[9,10] superconducting,[11,12] to magnetic,[13,14] as well as mechanical regimes.[15,16] One can expect combining multiple properties to explore novel applications.[17–19] Currently, the pursuing of wearable, intelligent, and implantable electronic systems has triggered the design and development of flexible and biocompatible materials for information collection, storage, and management.[20–23] The feature of 100% spin-polarized electrons at the Fermi level endows that 2D intrinsic half-metallic ferromagnets play an important role in spin-logic circuits in terms of energy efficiency and accuracy.[24–26] Thus, it is an alternative way to introduce spintronics to the realm of the flexible device to improve the performance of the device.

To date, most half-metals are transition metal oxides,[27,28] sulfides,[29] double perovskites,[30,31] or Heusler alloys.[32] However, these compounds usually have large stiffness which are not favored by flexible devices. The recent experimental realization of monolayer CrI_3 and few-layer $Cr_2Ge_2Te_6$,[33,34] has stimulated the research of 2D magnets. There are some encouraging theoretical progresses made in recent years, such as g-C_3N_4, $MnPSe_3$, CrN, GaSe, Cr_3X_4 (X = S, Se, Te), MO (M = Ga, In), Mn_3X_4 (X = S, Se, Te),[35–43] doped graphene nanoribbons,[44] and doped GaSe.[40] Among them, the monolayer CrN attracts our attention because it has two stable phases (square and hexagon) and both phases show simple structures and FM half-metallicity with relatively high Curie temperature, as well as good biocompatibility.[37,38,45] However, to our knowledge, researches on the flexibility and the survival of its exceptional properties under strains, which are crucial to the practical applications, are still lacking. Moreover, the Curie temperature has been proposed to be high based on a 2D Ising model, in which the super-exchange interaction and the magnetic anisotropy energy have not been considered. However, these two parameters influence the Curie temperature significantly.[46–49] Thus, the Heisenberg model is preferred to explore how these parameters influence the Curie temperature.

In this work, we explore a monolayer CrN in a square lattice as a binary half-metallic ferromagnet with ultra-low Young's modulus, large critical strain, and high Curie temperature by performing first-principles calculations based on den-

*Project supported by the National Natural Science Foundation of China (Grant No. 61888102), the National Key Research and Development Program of China (Grant No. 2016YFA0202300), and the Strategic Priority Research Program of the Chinese Academy of Sciences (Grant No. XDB30000000).

†Corresponding author. E-mail: zhangyanfang@ucas.ac.cn

© 2021 Chinese Physical Society and IOP Publishing Ltd

sity functional theory. We first present that the bulk CrN in a square lattice is only 68 meV/atom above hull by using a convex hull analysis of formation enthalpy. The monolayer CrN is proved to be a soft material with superior mechanical flexibility benefit from its ultra-low Young's modulus and large critical strain. The ferromagnetic half-metallicity is well retained under various strains. We further demonstrate that the half-metallicity and ferromagnetism are originated from the splitting of Cr-d orbitals in the CrN square crystal field, Cr–N bonding interaction, and Cr–Cr bonding interaction. Based on a Heisenberg model, we find that the monolayer CrN is a ferromagnet with high Curie temperature far above room temperature. All these intriguing features endow the monolayer CrN with exceptional potentials in nanoscale flexible devices and spintronic applications, and should attract experimentalists' attention to realize it in real devices.

2. Calculation method

All density functional theory (DFT) calculations were performed using density functional theory within projector-augmented wave (PAW) potentials[50,51] as implemented in the VASP code.[52,53] A vacuum slab of 20 Å and a plane-wave basis set with an energy cutoff of 520 eV were used. An $8\times8\times1$ Γ point centered k-mesh was applied to sample the Brillouin zone. GGA+U was employed to optimize the geometric structures,[54] where the U value was referred to Wang *et al.*'s work.[55] The structures were fully relaxed until energy and force were converged to 10^{-8} eV and 0.001 eV/Å, respectively. The phase diagram was calculated using the GGA+U method at 0 K. The compounds are all in stable structures obtained from the Materials Project database.[56] Their formation energies are calculated by the following formula:

$$\Delta E = \frac{E(A_xB_y) - xE(A) - yE(B)}{x+y},$$

where $E(A_xB_y)$ is the total energy of A_xB_y bulk material, $E(A)$ and $E(B)$ are the chemical potentials of elements A and B, respectively.

3. Results and discussion

The crystal structure of the monolayer CrN is displayed in Fig. 1(a). CrN consists a single layer of Cr atoms and N atoms in the form of a square lattice. The lattice has a D_{4h} point group with a lattice constant around 4.02 Å. A convex hull analysis of formation enthalpy was performed to look for the most stable phase. Three different phases of CrN were considered. One phase is a square lattice with a planar structure. The other two phases are both hexagonal phases, while one is a planar structure and the other is a sandwich structure.[56] Different magnetic configurations were considered to find the ground states for the three different phases. Then the total energies of the ground states were used to get the formation enthalpy. The phase diagram is plotted as Fig. 1(b). The formation energy of the square phase is 68 meV/atom higher (the red square in Fig. 1(b)) than that of the most stable phase, while the hexagonal phase is 211 meV/atom higher (the blue hexagon). The relatively small energy difference with the most stable one suggests that there is a high probability to fabricate the square phase CrN by using molecular beam epitaxy method.[56–58]

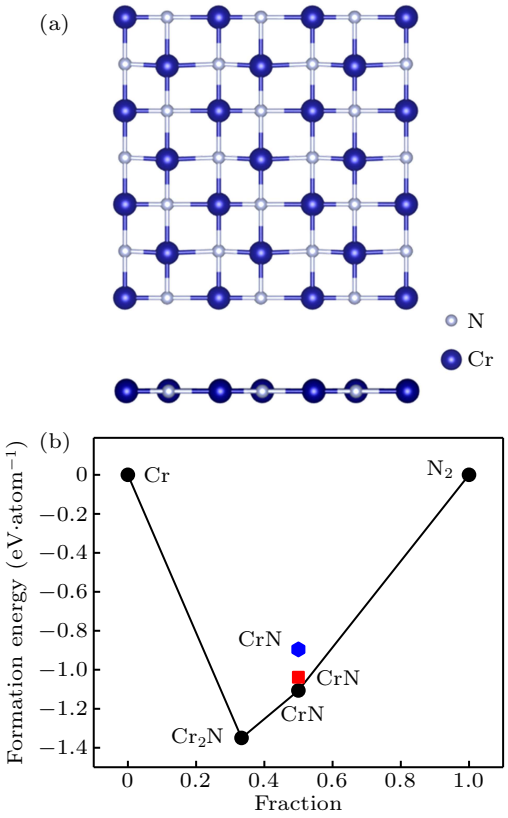


Fig. 1. Geometric structure of monolayer CrN (a) and the convex hull phase diagram of the Cr–N compounds (b).

The linear elastic constants of the monolayer CrN in the ferromagnetic ground state are calculated to further examine the mechanical stability. Based on the density functional perturbation theory (DFPT) method, the 2D linear elastic constants are as follows: $C_{11} = 117.07\ \mathrm{N\cdot m^{-1}}$, $C_{22} = 117.07\ \mathrm{N\cdot m^{-1}}$, $C_{12} = 62.68\ \mathrm{N\cdot m^{-1}}$, and $C_{44} = 7.19\ \mathrm{N\cdot m^{-1}}$. Since the stability criteria for a square 2D lattice[59] are $C_{11} > 0$, $C_{44} > 0$, and $C_{11} > |C_{12}|$, the monolayer CrN is obviously stable. Furthermore, the in-plane Young's modulus and Poisson's ratio are evaluated to analyze the mechanical properties of the monolayer CrN. The Young's modulus can be expressed as

$$E(\theta) = \frac{C_{11}C_{22} - C_{12}^2}{C_{11}s^4 + C_{22}c^4 + \left(\dfrac{C_{11}C_{22} - C_{12}^2}{C_{44}} - 2C_{12}\right)c^2s^2}.$$

The Poisson's ratio is

$$\nu(\theta) = -\frac{\left(C_{11}+C_{22}-\dfrac{C_{11}C_{22}-C_{12}^2}{C_{44}}\right)c^2s^2 - C_{12}(c^4+s^4)}{C_{11}s^4 + C_{22}c^4 + \left(\dfrac{C_{11}C_{22}-C_{12}^2}{C_{44}} - 2C_{12}\right)c^2s^2},$$

where θ is the angle relative to the positive x direction in the square lattice, $c = \cos\theta$, and $s = \sin\theta$. Figures 2(a) and 2(b) present the Young's modulus and the Poisson's ratio. The lowest Young's modulus is around 27 $\mathrm{N\cdot m^{-1}}$, together with the large Poisson's ratio (ranging from 0.54 to 0.85), demonstrating that the monolayer CrN is a promising material for flexible and stretchable electronic devices.

The total energies versus different values of strain are plotted in Fig. 2(c). One can expect that compressive strains induce similar structure changes under tensile strains due to the symmetry of the monolayer CrN. In addition, the change is asymmetric for compressive and tensile strains. For example, the monolayer CrN under a compress strain of 10% in x direction corresponds to that under a tensile strain of 25% in x direction, exhibiting a distorted hexagonal structure. Thus, only tensile strains are discussed in this work. There is one transition point labeled in red. The transition point corresponds to the break of one Cr–N bond, resulting in the transition of the monolayer CrN from a square lattice to a distorted hexagonal lattice, which is in accordance with two different phases of monolayer CrN.[37,38] There should be another peak referring to the crack of the monolayer hexagonal CrN, which is not discussed here. Figure 2(d) gives the crystal structures under different strains. It clearly shows that the Cr–N bonds break at strain 16%, forming a distorted hexagonal lattice (the second structure in Fig. 2(d)). Moreover, the structure with a 30% tensile strain (the last one in Fig. 2(d)) is a monolayer CrN in a hexagonal lattice under a compressive strain of 8%. When the tensile strain reaches 41%, a monolayer CrN in a hexagonal lattice without strain can be obtained. Considering that both two phases of monolayer CrN show ferromagnetic half-metallic behavior, the monolayer CrN is a promising material which can be used in flexible, stretchable, and biocompatible devices.

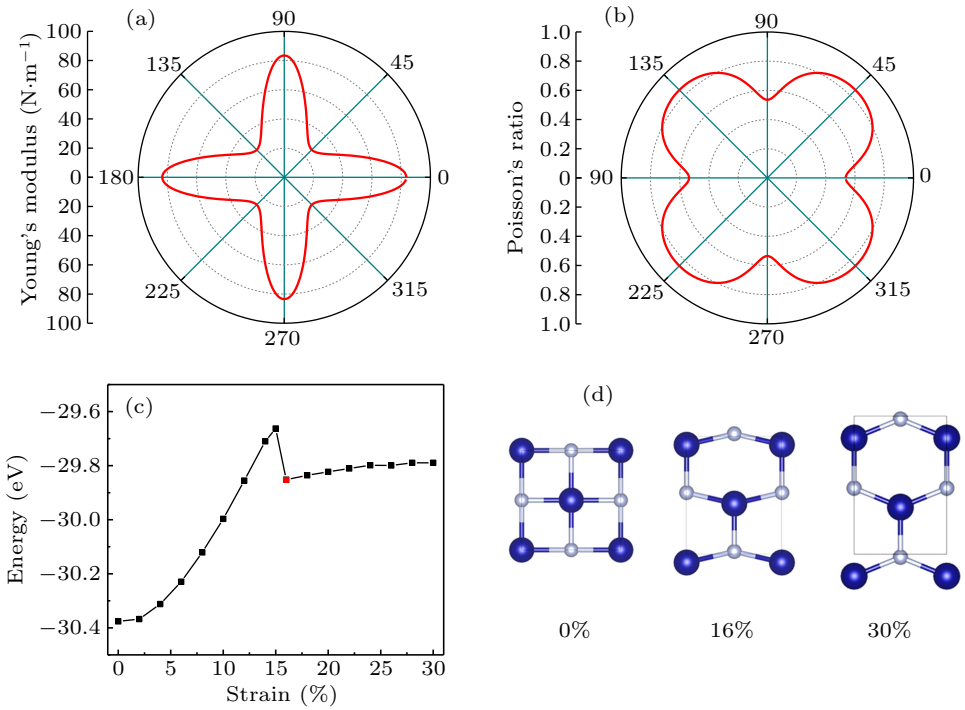


Fig. 2. Mechanic properties of the monolayer CrN. Polar diagrams for the (a) Young's modulus and (b) Poisson's ratio. (c) Total energy variation respect to strain. (d) Crystal structures at various strains.

The very low Young's modulus inspired us to explore the robustness of strain effect on the electronic properties of the monolayer CrN, which is of great significance for its potential application in flexible spintronic devices. As is shown in Fig. 3, the half-metallic ferromagnetism is well preserved under axial strains ranging from −4% to 4%. The value of the band gap has a linear relationship with the axial strain. Under compressive strains, the band gap increases from 2.07 eV to 2.36 eV as the strain decreases from −4% to −1%. The band gap further increases to 2.52 eV when the tensile strain increases to 4%.

In order to elucidate the half-metallicity of CrN, the projected densities of states (PDOS) on Cr atom are calculated, as can be seen in Fig. 4(a). Due to the exchange interaction, only α-spin channels are occupied while β-spin channels are empty for the Cr-d orbitals except for Cr-$d_{x^2-y^2}$ orbital. The α-spin channel of Cr-d_{xy} orbital is only partially occupied, thus making the CrN monolayer a half metal. This behavior can be

further explained by analyzing crystal field splitting and bond interactions as shown in Fig. 4(b). For the monolayer CrN, the Cr atom is surrounded by four nearest neighboring N atoms, forming a square lattice. Under a square planar crystal field without considering the bond interaction, the five Cr-d orbitals have a 2-1-1-1 splitting. The sequence of the five orbitals, according to their energy sites from the lowest to the highest one, is the degenerate d_{xz} and d_{yz} orbitals, d_{z^2} orbital, d_{xy} orbital, and $d_{x^2-y^2}$ orbital. Considering the bond interaction of Cr-d orbitals with the orbitals of neighboring atoms, the orbitals would further split into bonding and antibonding states. The $d_{x^2-y^2}$ orbital of Cr atom has the largest bond splitting due to the largest orbital overlap with the p_x (and p_y) orbital of its nearest-neighboring N atoms. The d_{xy} orbital has the next-largest bonding splitting due to the next-nearest neighboring Cr–Cr interactions. This qualitative analysis matches the PDOS on Cr well, and can be used in other similar structures.

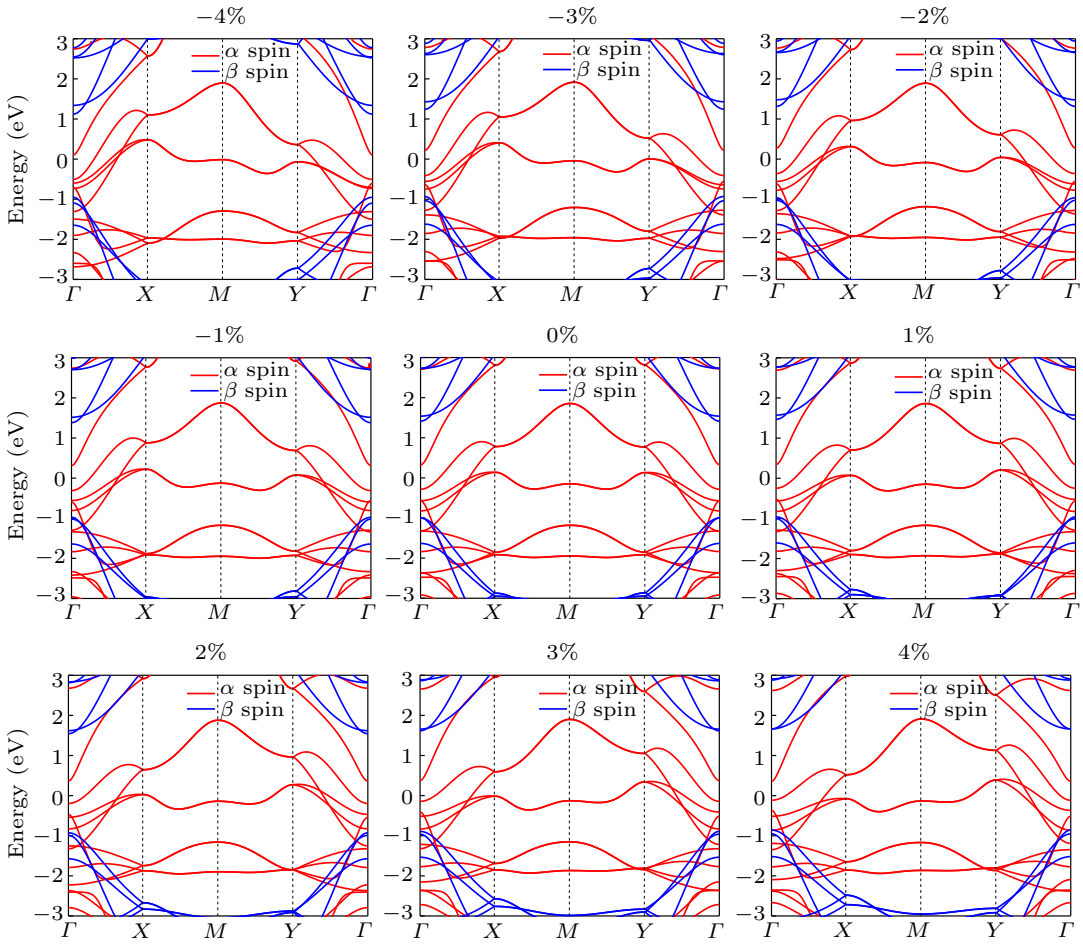


Fig. 3. Electronic structures of the monolayer CrN without strain and with compressive/tensile strains (from −4% to 4%).

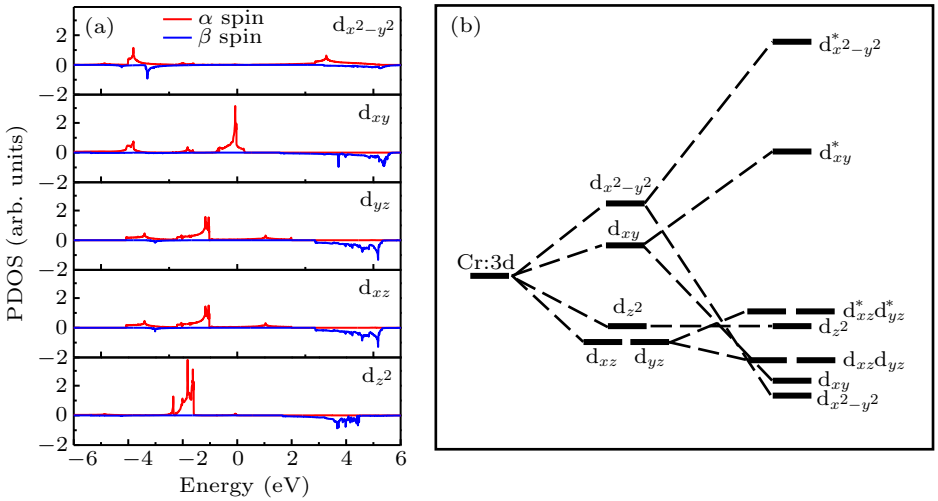


Fig. 4. Origins of the half metallicity. (a) Projected density of states on Cr-d orbitals. (b) Schematic representation of Cr-d orbital splitting.

Since Curie temperature (T_C) is a key feature for ferromagnetic materials, we then evaluate the T_C by performing Monte Carlo (MC) simulations based on a 2D Heisenberg Hamiltonian model. A four-state mapping analysis[60] is applied to extract the magnetic exchange interactions. The Heisenberg Hamiltonian model is defined as

$$\hat{H} = \sum_{i<j} J_{i,j} \boldsymbol{S}_i \cdot \boldsymbol{S}_j + \sum_i A(S_i^z)^2,$$

where $J_{i,j}$ describes the exchange coupling between two different Cr atoms at sites i and j. Two sets of J values are considered here (Fig. 5(a)). One corresponds to the nearest-neighboring Cr atoms, and the other one is the coupling between the secondary-nearest-neighboring Cr atoms. A and $(S_i^z)^2$ are the single-ion anisotropy parameter and the component of S_i along the z direction, respectively.

A 4×4 supercell is used to calculate the J related total energy of different magnetic configurations. We set different magnetic configurations (↑↑, ↑↓, ↓↑, ↓↓) of two Cr atoms and keep the spins of all the other Cr atoms in the same z-direction when estimating their exchange coupling interaction. The magnetic configurations for J_2 calculations are provided in Figs. 5(a)–5(c) as an example. The total energies are written as follows:

$$\begin{aligned}
E_1 &= J_{ij}S^2 + K_iS + K_jS + E_{\text{other}}S + E_0,\\
E_2 &= -J_{ij}S^2 + K_iS - K_jS + E_{\text{other}}S + E_0,\\
E_3 &= -J_{ij}S^2 - K_iS + K_jS + E_{\text{other}}S + E_0,\\
E_4 &= J_{ij}S^2 - K_iS - K_jS + E_{\text{other}}S + E_0,
\end{aligned}$$

in which the first three terms correspond to the exchange coupling interaction between the i-th and the j-th Cr atoms, among the i-th and the other Cr atoms, and among the j-th and the other Cr atoms, respectively. E_{other} and E_0 are the exchange coupling interaction among other Cr atoms and the energy unrelated to the exchange coupling interaction, respectively. Thus, the exchange coupling interaction between the i-th and j-th Cr atoms is $J_{ij} = \frac{E_1+E_4-E_2-E_3}{4S^2}$.

The J_1 and J_2 exchange coupling parameters for monolayer CrN are obtained by computing the above equation. The relative total energies for different magnetic configurations are 0 meV (E_1), 163.6 meV (E_2, E_3), 239.1 meV (E_4 for J_1), and 79.6 meV (E_4 for J_2), respectively. The J_1 and J_2 parameters are calculated to be −9.8 meV and −27.5 meV, respectively. The easy axis is along z-direction with an anisotropy energy parameter A of −0.45 meV. The relatively large J_2 parameter and the large magnetic moment ($3\mu_B$ per Cr atom) suggest a high T_C. From the variation of the average magnetic moment per Cr atom with respect to temperatures (Fig. 5(d)), it is easy to see that the estimated T_C is far above room temperature. It is important to note that the J_2 originated from the super-exchange interaction is larger than the J_1 derived from the direct-exchange interaction. This means that the super-exchange interaction contributes dominantly to the FM arrangement of monolayer CrN. It should be the reason that the predicted Curie temperature is higher than that in Wang's work.[37]

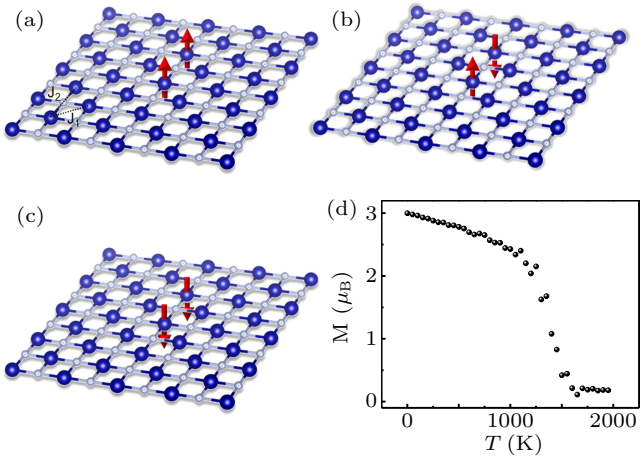


Fig. 5. Configurations with different magnetic ordering and Monte Carlo simulations. (a) Configuration with ↑↑ magnetic ordering. J_1 and J_2 are the Heisenberg exchange coupling between the nearest and the second-nearest neighbors, respectively. (b) Configuration with ↑↓ or ↓↑ magnetic ordering. (c) Configuration with ↓↓ magnetic ordering. (d) Temperature-dependent average magnetic moment per Cr atom based on Monte Carlo simulations.

It is worth noting that the magnetic mechanism is complicated, including but not limited to the hopping interaction, the on-site coulomb interaction, the orbital characteristics, and the charge states. The J terms in the Heisenberg model are a balance between the hopping interaction and the on-site coulomb interaction. The relatively large J_2 can be explained by the strong hybridization between the p orbitals of the N atoms and the $d_{x^2-y^2}$ orbitals of the Cr atoms due to the symmetry of the CrN monolayer. Despite the simplicity of the Heisenberg Hamiltonian adopted here, similar models have been proved to provide accurate results for the T_C in complex magnetic materials (e.g., multiferroic oxide perovskites[13,61,62]).

4. Conclusion

In summary, the monolayer CrN material in a square lattice is explored as a promising binary half-metal ferromagnet with ultra-low Young's modulus and large critical strain for flexible, stretchable, and biocompatible electronics. The half-metallicity is well preserved under various strains. The ferromagnetism and the half-metallicity are originated from the splitting of Cr-d orbitals in the CrN square crystal field, the bonding interaction between Cr–N, and that between Cr–Cr atoms. Interestingly, the super-exchange interaction is superior to the direct-exchange interaction. The Curie temperature is estimated to be higher than 1000 K based on the Heisenberg model. The high probability to be fabricated, the remarkable

mechanical, electrical, and magnetic properties deserve extensive experimental exploration.

References

[1] Novoselov K S, Geim A K, Morozov S V, Jiang D, Zhang Y, Dubonos S V, Grigorieva I V and Firsov A A 2004 *Science* **306** 666

[2] Elias C, Valvin P, Pelini T, Summerfield A, Mellor C J, Cheng T S, Eaves L, Foxon C T, Beton P H, Novikov S V, Gil B and Cassabois G 2019 *Nat. Commun.* **10** 2639

[3] Radisavljevic B, Radenovic A, Brivio J, Giacometti V and Kis A 2011 *Nat. Nanotech.* **6** 147

[4] Chhowalla M, Jena D and Zhang H 2016 *Nat. Rev. Mater.* **1** 16025

[5] Novoselov K S, Geim A K, Morozov S V, Jiang D, Katsnelson M I, Grigorieva I V, Dubonos S V and Firsov A A 2005 *Nature* **438** 197

[6] Zhang Y F, Pan J B, Banjade H, Yu J, Lin H, Bansil A, Du S X and Yan Q M 2020 *Nano Res.* **14** 584

[7] Ashton M, Gluhovic D, Sinnott S B, Guo J, Stewart D A and Hennig R G 2017 *Nano Lett.* **17** 5251

[8] Wu Q, Zhang Y, Zhou Q, Wang J and Zeng X C 2018 *J. Phys. Chem. Lett.* **9** 4260

[9] Briggs N, Bersch B, Wang Y, Jiang J, Koch R J, Nayir N, Wang K, Kolmer M, Ko W, De La Fuente Duran A, Subramanian S, Dong C, Shallenberger J, Fu M, Zou Q, Chuang Y W, Gai Z, Li A P, Bostwick A, Jozwiak C, Chang C Z, Rotenberg E, Zhu J, van Duin A C T, Crespi V and Robinson J A 2020 *Nat. Mater.* **19** 637

[10] Ji Q Q, Li C, Wang J L, Niu J J, Gong Y, Zhang Z P, Fang Q Y, Zhang Y, Shi J P, Liao L, Wu X S, Gu L, Liu Z F and Zhang Y F 2017 *Nano Lett.* **17** 4908

[11] Bekaert J, Petrov M, Aperis A, Oppeneer P M and Milosevic M V 2019 *Phys. Rev. Lett.* **123** 077001

[12] Yu Y, Ma L, Cai P, Zhong R, Ye C, Shen J, Gu G D, Chen X H and Zhang Y 2019 *Nature* **575** 156

[13] Cazorla C and Íñiguez J 2018 *Phys. Rev. B* **98** 174105

[14] Jiang S W, Li L Z, Wang Z F, Mak K F and Shan J 2018 *Nat. Nanotech.* **13** 549

[15] Sun Y F, Pan J B, Zhang Z T, Zhang K N, Liang J, Wang W J, Yuan Z Q, Hao Y K, Wang B L, Wang J W, Wu Y, Zheng J Y, Jiao L Y, Zhou S Y, Liu K H, Cheng C, Duan W H, Xu Y, Yan Q M and Liu K 2019 *Nano Lett.* **19** 761

[16] Liu K and Wu J Q 2016 *J. Mater. Res.* **31** 832

[17] Duerloo K A N, Li Y and Reed E J 2014 *Nat. Commun.* **5** 4214

[18] Wu W Z, Wang L, Yu R M, Liu Y Y, Wei S H, Hone J and Wang Z L 2016 *Adv. Mater.* **28** 8463

[19] Lin P, Zhu L P, Li D, Xu L, Pan C F and Wang Z L 2018 *Adv. Funct. Mater.* **28** 1802849

[20] Akinwande D, Petrone N and Hone J 2014 *Nat. Commun.* **5** 5678

[21] Liu Y, Pharr M and Salvatore G A 2017 *ACS Nano* **11** 9614

[22] Huang S Y, Liu Y, Zhao Y, Ren Z F and Guo C F 2019 *Adv. Funct. Mater.* **29** 1805924

[23] Jiang J, Bitla Y, Huang C W, Do T H, Liu H J, Hsieh Y H, Ma C H, Jang C Y, Lai Y H, Chiu P W, Wu W W, Chen Y C, Zhou Y C and Chu Y H 2017 *Sci. Adv.* **3** e1700121

[24] de Groot R A, Mueller F M, Engen P G v and Buschow K H J 1983 *Phys. Rev. Lett.* **50** 2024

[25] Park J H, Vescovo E, Kim H J, Kwon C, Ramesh R and Venkatesan T 1998 *Nature* **392** 794

[26] Wolf S A, Awschalom D D, Buhrman R A, Daughton J M, von Molnár S, Roukes M L, Chtchelkanova A Y and Treger D M 2001 *Science* **294** 1488

[27] Schwarz K 1986 *J. Phys. F: Met. Phys.* **16** L211

[28] Ji Y, Strijkers G J, Yang F Y, Chien C L, Byers J M, Anguelouch A, Xiao G and Gupta A 2001 *Phys. Rev. Lett.* **86** 5585

[29] Xie W, Liu B and Pettifor D G 2003 *Phys. Rev. B* **68** 134407

[30] Kobayashi K I, Kimura T, Sawada H, Terakura K and Tokura Y 1998 *Nature* **395** 677

[31] Liu Y P, Fuh H R and Wang Y K 2012 *J. Phys. Chem. C* **116** 18032

[32] Winterlik J, Fecher G, Naghavi S S and Felser C 2011 *Phys. Rev. B* **83** 184428

[33] Gong C, Li L, Li Z, Ji H, Stern A, Xia Y, Cao T, Bao W, Wang C, Wang Y, Qiu Z Q, Cava R J, Louie S G, Xia J and Zhang X 2017 *Nature* **546** 265

[34] Huang B, Clark G, Navarro-Moratalla E, Klein D R, Cheng R, Seyler K L, Zhong D, Schmidgall E, McGuire M A, Cobden D H, Yao W, Xiao D, Jarillo-Herrero P and Xu X 2017 *Nature* **546** 270

[35] Du A, Sanvito S, Sanvito S and Smith S C 2012 *Phys. Rev. Lett.* **108** 197207

[36] Li X, Wu X and Yang J 2014 *J. Amer. Chem. Soc.* **136** 11065

[37] Zhang S, Li Y, Zhao T and Wang Q 2014 *Sci. Rep.* **4** 5241

[38] Kuklin A V, Kuzubov A A, Kovaleva E A, Mikhaleva N S, Tomilin F N, Lee H and Avramov P V 2017 *Nanoscale* **9** 621

[39] Modarresi M, Mogulkoc A, Mogulkoc Y and Rudenko A N 2019 *Phys. Rev. Appl.* **11** 064015

[40] Cao T, Li Z and Louie S G 2015 *Phys. Rev. Lett.* **114** 236602

[41] Zhang X, Wang B, Guo Y, Zhang Y, Chen Y and Wang J 2019 *Nanoscale Horiz.* **4** 859

[42] Meng R, Houssa M, Iordanidou K, Pourtois G, Afanasiev V and Stesmans A 2020 *Phys. Rev. Mater.* **4** 074001

[43] Chen Z, Fan X, Shen Z, Luo Z, Yang D and Ma S 2020 *J. Mater. Sci.* **55** 5696

[44] de Vries E K, Kamerbeek A M, Koirala N, Brahlek M, Salehi M, Oh S, van Wees B J and Banerjee T 2015 *Phys. Rev. B* **92** 201102

[45] Liu J Y, Sun Q, Kawazoe Y and Jena P 2016 *Phys. Chem. Chem. Phys.* **18** 8777

[46] Gong C and Zhang X 2019 *Science* **363** eaav4450

[47] Torelli D, Thygesen K S and Olsen T 2019 *2D Mater.* **6** 045018

[48] Wang B, Zhang Y, Ma L, Wu Q, Guo Y, Zhang X and Wang J 2019 *Nanoscale* **11** 4204

[49] Wang B, Zhang X, Zhang Y, Yuan S, Guo Y, Dong S and Wang J 2020 *Mater. Horiz.* **7** 1623

[50] Blöchl P E 1994 *Phys. Rev. B* **50** 17953

[51] Kresse G and Joubert D 1999 *Phys. Rev. B* **59** 1758

[52] Kresse G and Furthmüller J 1996 *Phys. Rev. B* **54** 11169

[53] Kresse G and Furthmüller J 1996 *Comput. Mater. Sci.* **6** 15

[54] Dudarev S L, Botton G A, Savrasov S Y, Humphreys C J and Sutton A P 1998 *Phys. Rev. B* **57** 1505

[55] Wang L, Maxisch T and Ceder G 2006 *Phys. Rev. B* **73** 195107

[56] Jain A, Ong S P, Hautier G, Chen W, Richards W D, Dacek S, Cholia S, Gunter D, Skinner D, Ceder G and Persson K A 2013 *APL Mater.* **1** 011002

[57] O'Hara D J, Zhu T C, Trout A H, Ahmed A S, Luo Y K, Lee C H, Brenner M R, Rajan S, Gupta J A, McComb D W and Kawakami R K 2018 *Nano Lett.* **18** 3125

[58] Haastrup S, Strange M, Pandey M, Deilmann T, Schmidt P S, Hinsche N F, Gjerding M N, Torelli D, Larsen P M, Riis-Jensen A C, Gath J, Jacobsen K W, Mortensen J J, Olsen T and Thygesen K S 2018 *2D Mater.* **5** 042002

[59] Haastrup S, Strange M, Pandey M, Deilmann T, Schmidt P S, Hinsche N F, Gjerding M N, Torelli D, Larsen P M, Riis-Jensen A C, Gath J, Jacobsen K W, Mortensen J J, Olsen T and Thygesen K S 2019 *2D Mater.* **6** 048002

[60] Xiang H, Lee C, Koo H J, Gong X and Whangbo M H 2013 *Dalton Trans.* **42** 823

[61] Cazorla C and Íñiguez J 2013 *Phys. Rev. B* **88** 214430

[62] Cazorla C, Dieguez O and Iniguez J 2017 *Sci. Adv.* **3** e1700288